DEVELOPMENT OF CRUMPLED-BASED META-BIOMATERIALS AS BONE FILLING SUBSTITUENTS

BY
MARIKE FOKKER

TU Delft

DEVELOPMENT OF CRUMPLED-BASED META-BIOMATERIALS AS BONE FILLING SUBSTITUENTS

BY
MARIKE FOKKER

IN PARTIAL FULFILMENT OF THE REQUIREMENTS FOR THE DEGREE OF
MASTER OF SCIENCE
IN BIOMEDICAL ENGINEERING

AT THE **DELFT UNIVERSITY OF TECHNOLOGY**
TO BE DEFENDED ON JUNE 24TH, AT 14.00

THIS THESIS WILL HAVE EMBARGOED ACCESS FOR TWO YEARS AFTER GRADUATION.

STUDENT NUMBER:	4052277	
SUPERVISORS:	Dr. S. Janbaz	TU Delft
	Dr. N. Tümer	TU Delft
	Dr. M. Mirzaali	TU Delft
	Prof. Dr. A.A. Zadpoor	TU Delft
THESIS COMMITTEE:	Dr. S. Janbaz	TU Delft
	Dr. N. Tümer	TU Delft
	Dr. M. Mirzaali	TU Delft
	Prof. Dr. A.A. Zadpoor	TU Delft
	G. Radaelli, MSc	TU Delft

TU Delft

PREFACE

Bone defects are a common problem in healthcare today. When the damage is too extensive, the human body is not able to heal itself. Different solutions are available, but they all have limitations. Therefore, the search for a solution to overcome these limitations keeps going. In my graduation project, to conclude my master's degree in biomedical engineering, I had the pleasure of searching for a new way to build a scaffold that supports the human body to heal.

When Amir Zadpoor introduced me to this topic, I was intrigued. His idea to make a scaffold from crumpled-based elements was inspiring. However, I had no idea how and where to start. Luckily, Shahram Janbaz had a lot of inspiring ideas and helped me to experiment with different approaches. It took me a while, but eventually, I found a solid way to create a crumpled-based scaffold. Therefore I would like to thank Amir for introducing me to the topic, and Shahram for his never-ending ideas and inspiration.

Michiel Croes and Shahram Janbaz, thank you for your time and assistance during the µCT-scans. Additionally, I would like to thank all the people from the department for all the interesting conversations, new ideas, motivational comments, and much more. In particular, I would like to thank Françoise Bobbert for helping me design and optimize figures, Eline Kolken, Sebastien Callens, Teunis van Maanen and Nazli Tümer for the interesting discussions and new insights I gathered during those moments.

I also want to thank Amir and everybody from the department for their patience, understanding and support when times got rough for me. I really appreciate the space and time I've been given to get through it all. I came back a stronger person and I am very grateful for your willingness to help me finish this thesis. I also would like to thank Mohammad Mirzaali and Nazli Tümer for becoming my supervisors, when Shahram wasn't able to supervise anymore. You really helped me to finalize my thesis.

Last, but definitely not least, I would like to thank my family and friends who put up with me during this long and sometimes difficult road. I'm very grateful for all the support they gave me when I didn't know how to proceed. Their motivation was a crucial part of my journey.

Contents

1. INTRODUCTION

Bones are the basic building blocks of the human musculoskeletal system. The main function of the musculoskeletal system is to afford the body to move. Bones in particular give the body structure and stability to be able to function under loadbearing conditions [1]. Furthermore, bones protect other organs and tissues from external impact. During life, the bones will suffer from micro- or macro damages. In case of the micro-damage, the human body is usually able to repair it by itself. However, if the size of the damage is too large due to pathological diseases such as osteoporosis, cancer or tumour, it will not be self-healable, resulting in loss of tissue, loss of function, permanent disabilities and even death. In this case, replacing the damaged tissue (e.g. bone) would be unavoidable. Transplantation of autologous or allogeneic bone tissue is a frequently used treatment strategy, but resources are limited, especially for autologous bone transplantation [2]. Furthermore, harvesting autologous bone causes pain and sometimes nerve injury at the collection sites, while allogeneic bone could cause disease transfer [2]. As the costs for the procedure are high as well, this is not a concrete solution [2]. Other treatments, such as implants, medical devices or the use of drugs, are widely available, however, all are limited. These treatment strategies can't mimic the biological tissue structure and don't fully restore all the functionalities of the damaged tissue [1, 3]. Therefore other solutions to heal or replace the damaged tissue, without the limitation of availability or functionality should be studied.

Tissue engineering, in which new tissue is cultured to replace damaged tissue, could overcome the majority of the limitations in the treatments mentioned earlier. Cells of the patient himself will be used to develop new tissue by utilizing a three-dimensional (3D) porous scaffold, which includes all the functionalities of the damaged tissue, only without the limitation of availability [3]. In case of a bone tumour that needs to be removed, a scaffold can fill the void, the tumour left, and facilitate the reformation of bone tissue.
Porous scaffolds used for tissue engineering have to meet several criteria to result in a successfully engineered tissue [4]. First of all, the scaffold itself needs to be biocompatible and preferably biodegradable, to avoid inflammatory reactions and allow for the tissue to take over all the functionalities once fully grown [3-7]. Furthermore, the scaffold should provide the mechanical properties of the desired tissue during cultivation [3-7]. Lastly, the surface of the scaffold should permit and preferably stimulate cell adhesion and growth [3, 5, 6]. Porosity, size and density of the pores and surface to volume ratio are also other important parameters to allow cellular adhesion and growth, vascularisation and nutrient transportation [3, 5, 6]. Additionally, cell proliferation, orientation, morphology and signalling are influenced by the structure of the surface, in the same way as surrounding cells and the native extracellular matrix (ECM) influence a cell in its natural environment, through chemical and mechanical signals [6, 8-12].

Crumpling could be a very promising technique to meet all the criteria. In literature [13] multiple examples of potential crumpled-based materials have been mentioned. As shown in Figure 1-1-1, crumpled-based materials have multiple potential applications in various fields of expertise. The flexibility in many properties, such as porosity, strength, and stiffness, offers the crumpled-based material a way to obtain a wide range of properties. Crumpling could be used to sense pressure and strain [14] (Figure 1-1-1a), in lithium-ion batteries [15] (Figure 1-1-1b), to reduce the friction coefficient in lubricants [16] (Figure 1-1-1c), for dynamic control of surface wettability [17] (Figure 1-1-1d), for super flexibility in wood [18] (Figure 1-1-1e), in functionalizing the surface of a crumpled-based scaffold [9] (Figure 1-1-1f), or to adjust the cytoskeleton tensions by the curvature of the surface [19] (Figure 1-1-1g)

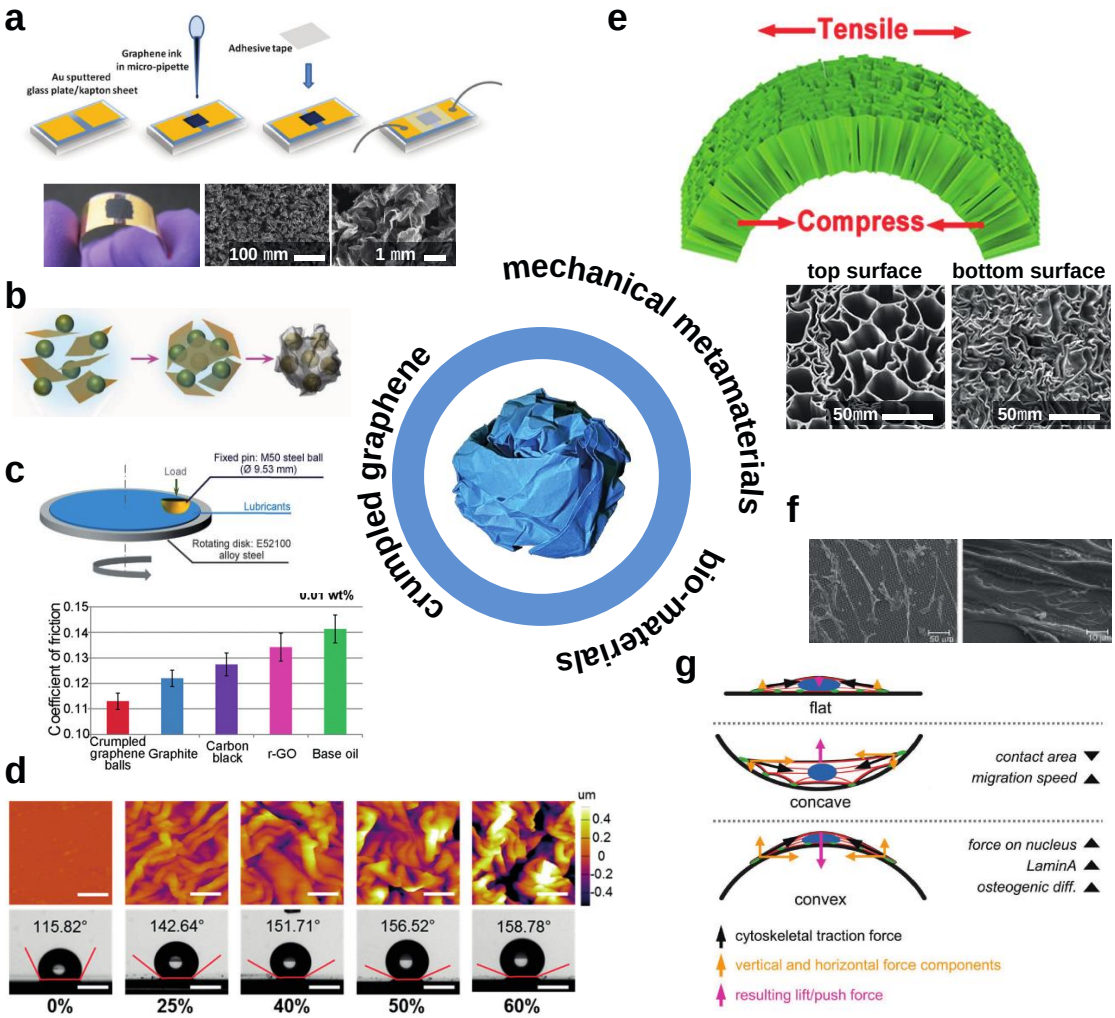

Figure 1-1-1: A selected overview of potential applications for the use of crumpled-based materials. ***a.*** *crumpled sheets of graphene oxide could be used for a robust sensation of pressure and strain.* ***b.*** *μ-meter sized graphene sheets can be used to encapsulate Si nano-particles in the process of evaporation of liquid droplets in lithium-ion batteries.* ***c.*** *Graphene crumpled balls could be used to reduce the friction coefficient of lubricants.* ***d.*** *Crumpled patterns of molybdenum disulfide on polystyrene substrate, realized through shrinkage of the polystyrene layer, could be used for dynamic control of surface wettability.* ***e.*** *a simple chemical treatment of in-natural wood could initiate super flexibility, as the μ-structure could be imitated artificially based on crumpling of planar materials.* ***f.*** *The pattern of cell adhesion could be adjusted by functionalizing the surface of crumpled-based scaffolds.* ***g.*** *The cytoskeleton tensions could be adjusted by the curvature of the surface.*

In our case the last two potential applications are exciting. In functionalizing the surface of a scaffold, topological or chemical cues are used to improve cell differentiation, cell orientation, cell proliferation and cell morphology. The surface enhancement techniques not only allow for optimizing the surface structure to support cell growth but inhibit the growth of bacteria as well [8]. This may be an attractive alternative for disinfectants or conventional antimicrobial agents which often leave a toxic residue. Several surface enhancement techniques are available. However, many techniques, such as nanolithography [20-22] or electron-beam induced deposition [23], are solely applicable to flat surfaces [20, 22, 24], which requires creating a scaffold starting from a flat surface. Origami based structures, structures that start as a 2D structure and shift into a three-dimensional structure, have been studied before [23-25]. With this

approach, a broad range of surface enhancement techniques could be used to optimize the surface, while ultimately a three-dimensional scaffold is obtained. However, the studied origami-based approaches result in a structured origami arrangement, in which a small defect could easily lead to substantial changes in the mechanical properties of the 3D scaffold [13, 26, 27]. To overcome this limitation, a more random approach such as crumpling could be used.

Crumpling is a 2D to 3D transformation, which results in a randomly folded structure, and therefore exhibits lower sensitivity to errors [13, 27-29]. As we reviewed the mechanical and morphological properties of crumpled materials in our former review paper [13], we learned that crumpled materials are well reproducible [13, 28, 29] and are known for a high porosity [13, 30-33], while presenting high strength due to the concentration of energy in the ridge network [13, 34, 35]. The ridge network grows when the material is further compressed. Therefore, the energy stored in the ridges will grow and the strength will become higher. This allows for tuning the strength of the material and matching it to the strength needed for the application [13, 29, 34, 35]. Our review also showed not only strength depends on the confinement ratio, but the Poisson's ratio as well [13, 29, 34, 35]. Crumpled materials are highly available, easy to produce and therefore cheap, maintaining robust mechanical properties [13, 26-28, 36].

As Bouaziz et al [29] showed, crumpled materials could be designed to exhibit auxetic behaviour. This means that when the material is stretched in the longitudinal direction it will become thicker in the perpendicular direction as well. This unexpected behaviour is common in many natural systems, such as skin, tendons and cancellous bone [37]. Auxetic materials are therefore interesting for multiple medical applications, such as stents, smart bandages and orthopaedic implants. The auxetic materials could mimic the cancellous bone and therefore prolong the lifespan of an implant [37].

Another interesting property of crumpled materials is relaxation, the dilatation of the crumpled membranes after the compressive load is removed [13, 28]. This property could be interesting to assemble multiple crumpled structures by unfolding and therefore tangling into each other and forming a scaffold. Relaxation itself is not strong enough. However, combined with a shape memory material (SMM), a material that can change its shape when exposed to the right stimuli (e.g. chemical, thermal, electro-chemical) [38-42], it could be viable. When a scaffold could be built out of small elements, it could be used to implant in a patient by minimal invasive (MI) surgery, to reduce damage to the body as a result of the surgery, resulting in less blood loss during surgery, faster recovery time with less pain and minimal scarring [43].

1.1 Research questions

In this thesis, I aim to design, fabricate and characterize crumpled-based meta-biomaterials as bone filling substituents. Toward this aim, I addressed the following research questions for a successful design of such crumple-based meta-biomaterials:

1. Can crumpling be used as a technique to create a porous scaffold in a reproducible way?
2. How to use smart materials (e.g., shape memory polymers) as a building block of crumpled-based meta-biomaterials, by making separate crumpled elements and combining them with the use of arbitrary shape changes?
3. Does the geometry of the separate elements, used to create the scaffold, influence the mechanical properties of the fabricated scaffold?
4. Does the initial porosity of the scaffold affect the mechanical and morphological properties?

2. Materials and Methods

Porous scaffolds were created by separate 3D printed crumpled elements, made of PolyLactic Acid (PLA), which is a shape memory polymer (SMP). Multiple elements were put in a confined space and activated by an external stimulus (heat) at a temperature above their glass transition. This causes the elements to reform to their former flat shape and therefore entangling to each other and forming a porous scaffold with a random microstructure. After creating the porous scaffolds, quasi-static compression mechanical tests were performed to determine their macroscopic mechanical properties. A selected group of porous scaffolds were scanned in a µCT-scanner to examine their morphological properties as well.

2.1 Element design and fabrication

Porous crumpled-based scaffolds were created by separate elements, which consist of a base and a corresponding number of arms. Four different base geometries have been included in this study: 1) triangle 2) square 3) pentagon and 4) circle, were used with three, four, five and six arms respectively. Additionally, the armlength (a) was varied between 8 and 16 mm with an increment of 4mm, to explore if this would affect the entanglement between the separate elements within a scaffold (Figure 2-1). The elements were designed in SolidWorks 2016 Education Edition 3D CAD software (Dassault Systemes, Waltham, USA). The width of the base geometry (wb), the width of the arms (wa), the length of the base (b), as well as the overall thickness of the elements (t) were kept constant for all the designs (Figure 2-1). Figure 2-1 shows the four different element geometries, as well as the measurements corresponding to the values specified in Table 2-1.

The material used for creating the elements was Polylactic Acid (PLA). This is a shape memory polymer (SMP), meaning the material can be programmed to memorize a permanent shape. When the material is deformed to a temporary shape, it will recover to the permanent shape once it is exposed to the right stimulus [38, 39, 44]. In PLA the stimulus that will trigger the material to recover to the permanent shape is heat. Furthermore, PLA is biocompatible as well as biodegradable [38, 44], easy to process, eco-friendly, and its mechanical, physical, chemical and microstructural properties can be modified, to create the most optimal set of properties for a specific application [38, 44-46]. Additionally, it has been shown that PLA can be used for drug release and stimulating tissue regeneration [44].

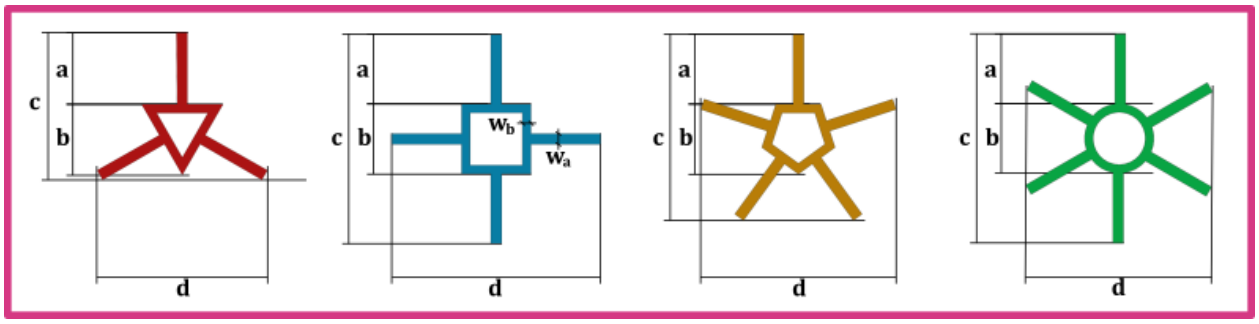

Figure 2-1: The four different element geometries consisting of a base geometry with a corresponding number of arms. In this figure, the measurements are shown corresponding to the values stated in Table 2-1.

Table 2-1: Measurement values of the different element designs.

	Total Number of Arms	b (mm)	a (mm)	c (mm)	d (mm)	Area (mm²)
Triangle	3	8	8	16.48	19.11	51.34
			12	22.48	26.03	65.85
			16	28.48	32.96	80.36
Square	4	8	8	24.00	24.00	67.97
			12	32.00	32.00	88.00
			16	40.00	40.00	108.00
Pentagon	5	8	8	21.32	22.40	72.27
			12	28.55	30.02	97.28
			16	35.78	37.62	122.26
Circle	6	8	8	24.00	21.41	82.13
			12	32.00	28.21	111.60
			16	40.00	35.14	141.60
w_b = 1.0 mm; w_a = 1.25 mm; thickness = 1.0 mm						

Figure 2-2: The process of creating a crumpled element a. Printing the elements with a FDM printer b. postprocessing the elements by removing the brim layer c. Heating the element by holding it in a waterbed of 90°C for 10 seconds d. crumpling the element by hand.

Figure 2-3: Recovery of a crumpled element to its permanent 2D shape in time, when submerged in water with a temperature of approximately 95°C.

Figure 2-2 shows the process leading to a crumpled element, starting with printing the designed elements with the use of a 3D printer based on fused deposition modelling (FDM) (Ultimaker, Geldermalsen, The Netherlands). Printing was done with a 0.4mm nozzle, a printing speed of 40 mm/s, a layer thickness of 0.1mm and a printing temperature of 210°C. For better adhesion to the print plate, a brim layer with a width of 8 mm was added (Figure 2-2a). After printing the elements needed to be separated and post processed by removing the brim layer, as shown in Figure 2-2b. This results in separate 2D elements. To crumple the elements, the properties of the SMP were used. A single element was placed in an aquarium, filled with water kept at a constant temperature of 90°C, for 10 seconds (Figure 2-2c). Subsequently, as shown in Figure 2-2d, the element was crumpled by randomly twisting the element manually, followed by rolling it between the fingers into a ball. Resulting in a crumpled element shown in Figure 2-2e.

The recovery of a crumpled element to its original 2D state is shown in Figure 2-3. A crumpled element was submerged in water with a temperature of approximately 95°C and was timed to know how long it would take to return to its original form. As shown in Figure 2-3, it took 3 seconds for the crumpled element to return to its original flat state.

2.2 SCAFFOLD DESIGN AND FABRICATION

*Figure 2-4: The process of creating a scaffold **a.** Multiple crumpled elements **b.** a specific number of crumpled elements were placed in a cylindrical holder **c.** The holder was closed with a top lid. In the holder, there are multiple holes to let the hot water flow through **d.** The holder was placed in a hot water bath of 90°C for 15 seconds **e.** After the scaffold was cooled down this is the end product.*

Scaffolds were made of multiple crumpled elements (Figure 2-4a). Each scaffold contained elements of only one design to be able to compare the different geometries. Scaffolds with different porosities were created by using different quantities of elements per scaffold. The porosity (Π) of the final crumpled-based porous scaffold was calculated according to [47-49]:

$$\Pi = 100\left(1 - \frac{\rho_s}{\rho_m}\right) = 100\left(1 - \frac{V_s/M_s}{V_m/M_m}\right) = 100\left(1 - \frac{M_s}{M_m}\right) = 100\left(1 - \frac{V_s}{V_m}\right) \qquad (2\text{-}1)$$

with ρ_s, V_s, M_s, ρ_m, V_m, M_m representing the density, volume and mass of respectively the scaffold and the material itself. The mass of the scaffolds is determined by weighing the elements on a Sartorius© 1801 balance before assembling them into a scaffold.
Primarily, scaffolds with a porosity of 80% were created. For each element design, three scaffolds were created. Subsequently, scaffolds with a porosity of 75% and 85% were created as well, however for those porosities only one scaffold per element design was made.

Multiple crumpled elements, variating from 14 to 62 elements, depending on the desired porosity and the geometry of the elements, were used to make one cylindrical scaffold with a height of 18 mm and a radius of 16 mm. After weighing the elements and determining the number of elements needed for a scaffold, the crumpled elements were placed in a holder. The holder is made of laser-cut plexiglass parts and consists of a bottom lid, a ring and a top lid. Small holes were created in all the elements of the holder to allow hot water to flow through for activation of the elements, 17 holes in the top and bottom lid each and 8 holes in the ring. Figure 2-4b shows the crumpled elements in the holder without the top lid. Figure 2-4c shows the complete holder. The holder with the elements is placed in the hot water bath (90°C) for 15 seconds (Figure 2-4d). This causes the crumpled elements to unfold. However, the space is limited, causing the elements to entangle as they all try to recover to their original flat shape. Subsequently, the holder was held under flowing cold water (17°C) to cool the elements down and fixate their shape, resulting in the creation of a porous crumpled-based scaffold (Figure 2-4e).

2.3 MECHANICAL TESTING

Figure 2-5: Different stages during the mechanical compression testing

Mechanical confined compression tests were performed on the crumple-based scaffolds. The scaffold was confined in the plexiglass ring which was part of the holder. A Lloyd Instruments LR 5K (Ametek inc.) mechanical testing machine with a 5kN load cell was used. The software used to control the machine and record the measurements (i.e., load, displacement, time) was Nexygen 3.0.
All scaffolds were compressed with a strain rate of 1 mm/min until a compression of 9mm was obtained, which corresponded with 50% of the original height of the scaffold causing a longitudinal strain of 0.5. The compression mechanical tests were displacement-controlled and axial load (F) due to the deflection of the porous scaffolds was measured. Sequentially the scaffold was unloaded with 1mm/min until the force reached zero. With these data, the stress-strain data were obtained. The axial stresses (σ) were defined as the ratio of the force (F) divided by the original cross-section area of the holder filling up the scaffold (πr^2) [28]:

$$\sigma = \frac{F}{\pi r^2} \qquad (2\text{-}2)$$

The longitudinal strains (ε) were calculated by:

$$\varepsilon = \frac{\Delta h}{h_0} \qquad (2\text{-}3)$$

In which Δh and h_0 represent the difference in height and the original height of the scaffold respectively.
The elastic stiffness (E) was determined by the slope of the linear regime of the stress-strain curves as:

$$E = \frac{\sigma}{\varepsilon} \qquad (2\text{-}4)$$

The initial elastic stiffness of the porous scaffold was determined at the small strain values (i.e., less than 0.05). The evolution of the elastic stiffness during the compression was also evaluated by calculating the elastic stiffness at different compression levels, with steps of 0.025 strain.

The mass of each scaffold (M_s) was determined by weighing the scaffold on a Sartorius© 1801 balance. The density of each scaffold was determined by dividing the mass of the scaffold (M_s) by the volume of the scaffold (V_s):

$$\rho = \frac{M_s}{V_s} \qquad (2\text{-}5)$$

The relative density (RD) was calculated by dividing the density of the scaffold (ρ) by the density of PLA (ρ_s):

$$RD = \frac{\rho}{\rho_s} \qquad (2\text{-}6)$$

To examine if initial density has any effect on the elastic stiffness at a given relative density, the graphs of the evolution of the elastic modulus for porous scaffolds with different initial densities were combined and compared.

Energy absorption (W) was another mechanical property that was calculated for each scaffold. It was defined as the area (numerical integration) under the stress-strain curve between two strain levels, initial strain (ε0) and final strain (εf) [50]:

$$W = \int_{\varepsilon_0}^{\varepsilon_f} \sigma(e)de \qquad (2\text{-}7)$$

2.4 MICRO CT SCANNING

*Figure 2-6: **a.** device used to manually compress the crumpled-based scaffolds in between scans **b.** Quantum FX micro-CT imaging system used for the non-destructive scanning of scaffolds **c.** Materialise Mimics software was used to render and reslice the Dicom files obtained by scanning the scaffolds with the micro-CT scanner **d.** Fiji ImageJ software together with the plugin BoneJ was used to define the morphological properties of the scaffolds.*

In addition to the mechanical testing, morphological features were investigated. This was done by scanning the crumpled-based scaffolds using a Quantum FX micro-computed tomography (µCT) imaging system (Quantum FX; PerkinElmer, Waltham, MA) to non-destructively evaluate their morphological features. µCT works based on capturing 2D planar x-ray images and reconstructing them into 3D models [28]. The 3D images were represented as a stack of 2D images with a spatial resolution of 80 µm. The operated tube voltage was 90 kV, the applied tube current was 180 mA and a 40 mm field of view was used.

In this study, three scaffolds, made from elements with a pentagonal base, but different armlengths were used for the visualization of the morphological features during progressive compressive tests. All scaffolds were scanned before the compression test, and at several stages during compression. The scaffolds were compressed in a device (PVC) shown in Figure 2-5, by turning the top and bottom in opposite directions by hand. Therefore the compression level of 50% was not reached in these samples. The highest compression level reached in this device was 58%.

The data derived from the µCT scanning contained a stack of 2D images stored in Digital Imaging and Communications in Medicine (DICOM) format. Those images were rendered with the use of Mimics software (Materialise N.V., Heverlee, Belgium). With the use of this program, the scaffolds were segmented and 3D reconstructed. The 3D images derived from the µCT scanner were tilted, which made them difficult to process. Therefore the images were corrected and levelled and resliced so calculations of several morphological properties were easier to perform.
Fiji; ImageJ 1.51h (Wayne Rasband National Institutes of Health, USA)[51] with plugin BoneJ [52] was used to determine the porosity and mean pore size of the scaffolds. An 8-bit image of the DICOM file was used to set a threshold, with the use of Li's Minimum Cross-Entropy thresholding method, to make the image

black and white, so the distinction between flakes and open space was easy to determine. The first thresholding value was 53, the second thresholding value was 255. Afterwards, a region of interest was set, so only the scaffold was taken into account, and not the surrounded device in which the scaffold was compressed. Then the plugin BoneJ was used to calculate trabecular spacing and volume fraction.

3. RESULTS

3.1 POROSITY

The scaffolds with a porosity of 80% had a mean porosity of 80.16% with a standard deviation of ±0.17%. The scaffolds with a porosity of 75% and 85% had a mean porosity of 74.91% and 84.99% respectively, with a standard deviation of ±0.18% for both.

3.2 MORPHOLOGICAL PROPERTIES

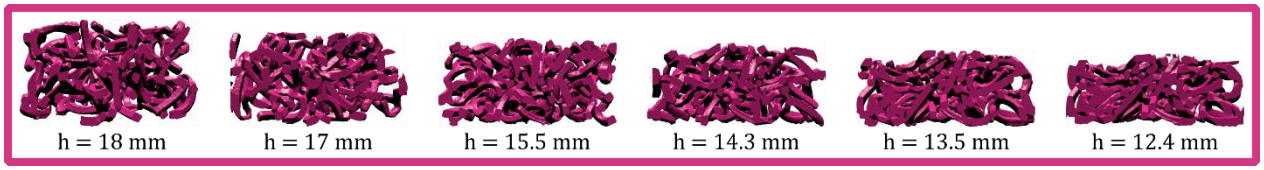

Figure 3-1: The longitudinal cross-sections of different stages during compression of a crumpled-based scaffold with a pentagon base and 8 mm arms and a starting porosity of 80%.

Crumpled-based scaffolds with a porosity of 80% made of elements with a pentagonal base, were used to study the morphological properties of the scaffolds. Figure 3-1 shows the longitudinal cross-section of a scaffold, made of elements with a pentagonal base geometry with arms of 8mm, at different stages during compression. As the height of the scaffold decreased the number of contacts grew. The scaffold became denser, as the spacing between elements decreased. No fraction was observed during compression, only densification (i.e., constantly increasing stress values) was observed.

Table 3-1: Measurements of the spacing between the elements, the mean strut thickness and the porosity before and after the compression of scaffolds made of elements with a pentagonal base and arms with a length of 8, 12 and 16 mm.

Crumpled -based Scaffold	Before/after compression	Mean pore size [mm]	STD pore size [mm]	Mean thickness [mm]	STD thickness [mm]	Porosity [%]
Pentagon 8 mm	Before	2.677	1.014	1.084	0.161	78.5
	After	1.750	0.747	1.043	0.184	68.1
Pentagon 12 mm	Before	2.823	1.197	1.184	0.176	75.3
	After	1.746	0.752	1.100	0.175	64.5
Pentagon 16 mm	Before	2.919	1.216	1.141	0.156	77.9
	After	1.891	0.826	1.078	0.208	64.8

Three different crumpled-based scaffolds, made of elements with a pentagonal base and three different arm lengths (i.e. 8, 12, and 16mm) were µCT-scanned at different stages during compression. In the course of the analysis of the µCT images, spheres were fitted into the pores before and after compression to determine the mean pore size at a certain degree of compression. Figure 3-2 shows a transversal cross-section of crumpled-based scaffolds before and after compression. From this figure, it becomes clear that the pore sizes are smaller after compression. Table 3-1 shows the values of the mean pore sizes. The mean pore size decreased when porosity decreased. The porosity before and after compression is also mentioned in Table 3-1. The scanned crumpled-based scaffolds were compressed by hand, with the use of a device shown in Figure 2-6, and therefore the porosity after compression is different in each scaffold. Table 3-1 shows only a small difference in the use of elements with 8-, 12- and 16-mm arms. To check the design of the crumpled-based scaffold, the thickness of the struts of the elements was measured as well. Table 3-1 shows the strut thickness is similar to the thickness we designed.

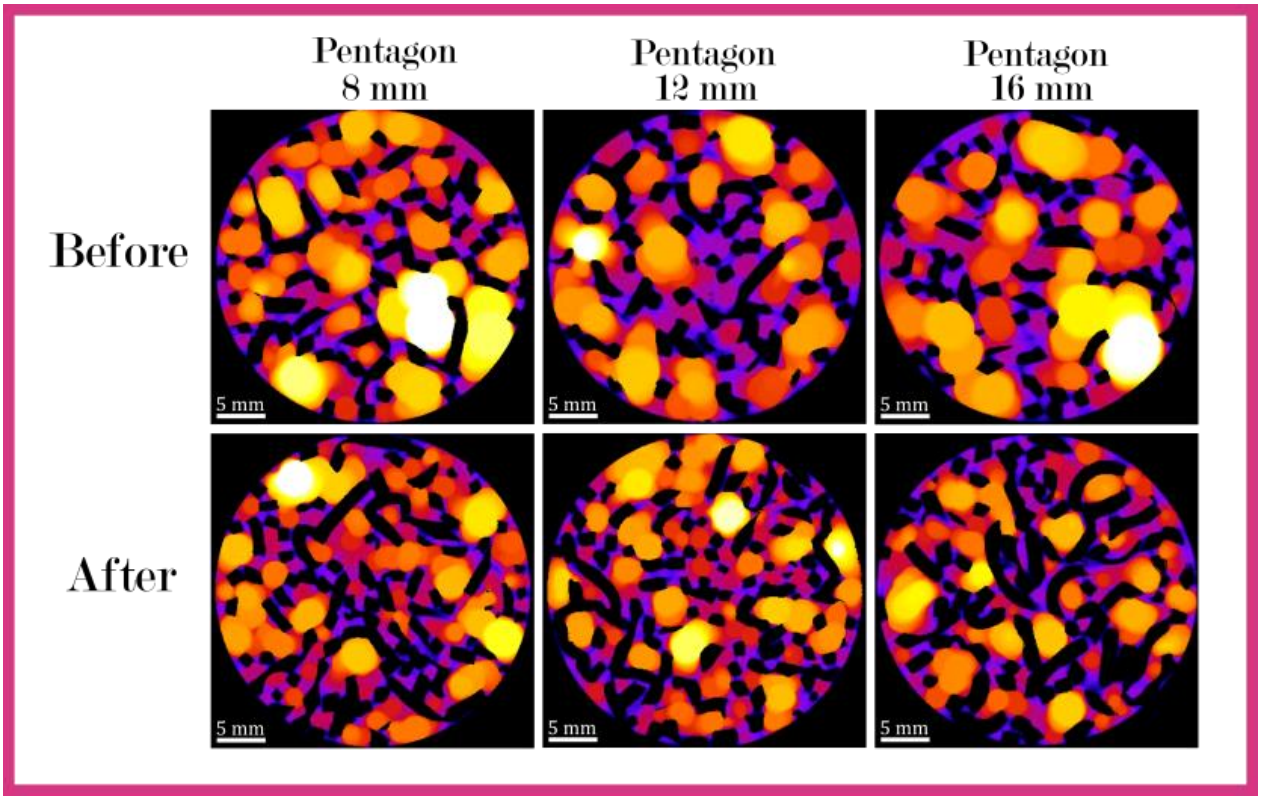

Figure 3-2: Transversal cross-sections of crumpled-based scaffolds made of elements with a pentagonal base and arm lengths of 8, 12 and 16 mm to visualize the pore sizes between the elements before and after compression.

3.3 MECHANICAL PROPERTIES

Crumpled-based scaffolds with three different porosities were used for mechanical testing. In total sixty scaffolds were subjected to the quasi-static compression loading until a strain of 50% was reached. None of the crumpled-based scaffolds were fractured during compression. In the group with a porosity of 80%, three scaffolds of each design were tested to verify the reproducibility of the test.

From Figure 3-3 it becomes clear that the curves per design were comparable. Therefore, only one scaffold per design was tested in the scaffold groups with the 75% and 85% porosities. The stress-strain curves derived from the compression tests were used to derive the initial elastic stiffness, the evolution of the elastic stiffness and the energy absorbed by the scaffold during the compression testing.

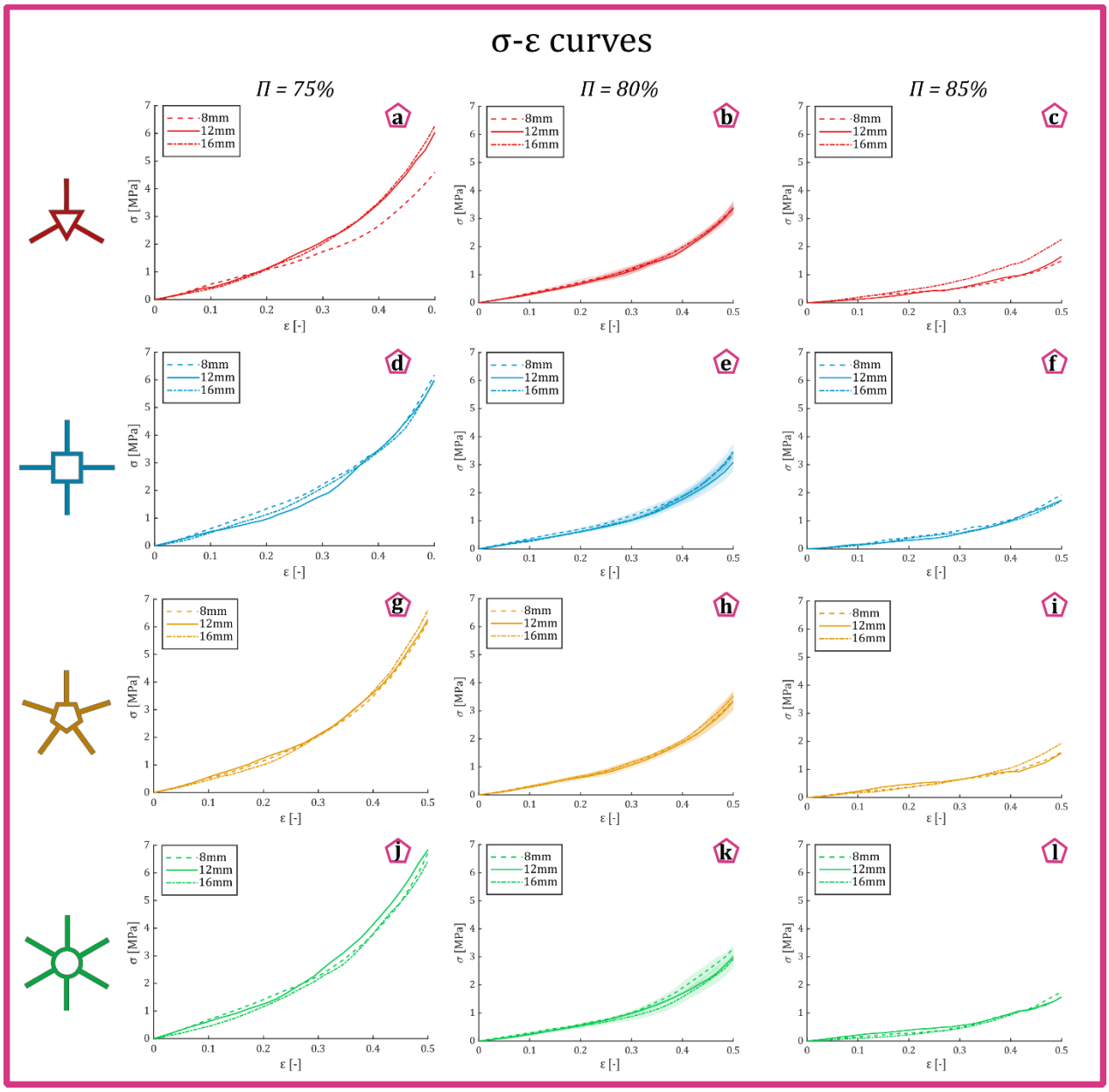

*Figure 3-3: Stress-strain curves derived from quasi-static compression tests with a compression rate of 1mm/min for crumpled-based scaffolds with porosity levels (Π) of 75%, 80%, and 85% composed of elements with the base geometry of triangle (**a.-c.**), square (**d.-f.**), pentagon (**g.-i.**) and circle (**j.-l.**) and with an arm length of 8 mm, 12 mm and 16 mm. In the group with a porosity of 80%, three different scaffolds were mechanically tested which means that three tests were performed for each combination of base geometry and armlength. In those stress-strain curves, the line shows the average and the coloured patch shows the standard deviation.*

The stress-strain diagrams derived from the compression tests (Figure 3-3) were similar to the stress-strain diagrams of entangled materials [53-57]. The stress-strain curves only showed an increase in the level of compaction, known as densification. During densification, the number of contacts between the elements increased while the porosity decreased, which caused a resistance toward more compression (Figure 3-3). This has resulted in the increase of the elastic stiffness when the load increased [58-60].

In the designs of the elements, a difference was made in the base geometry and the number and length of the extending arms. Neither the base geometry nor the number and length of the arms seems to influence the overall stress-strain behaviour of the crumpled-based scaffolds (Figure 3-3). Only the porosity of the crumpled-based scaffold showed to have a noticeable impact. The lower the porosity the higher the stresses were during compression (Figure 3-3).

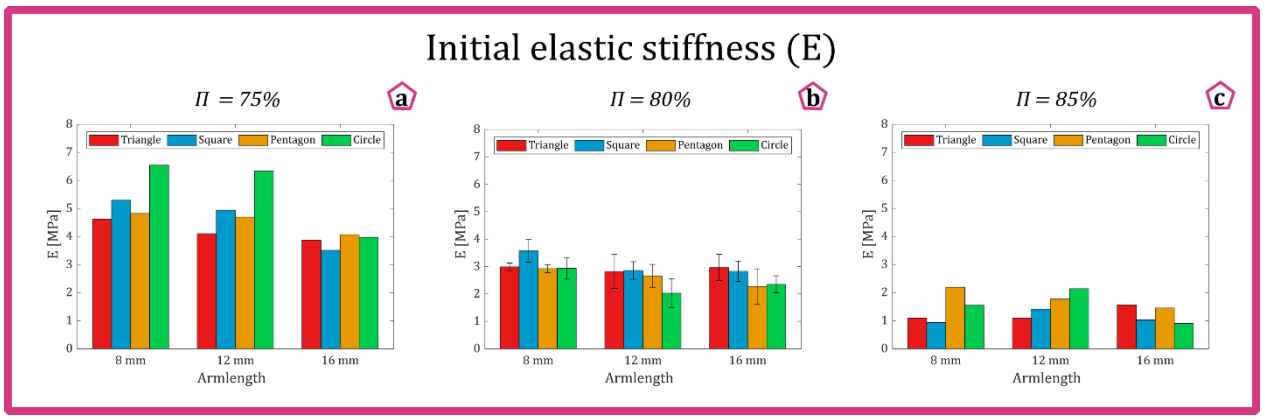

*Figure 3-4: The initial elastic stiffness (E) calculated from the stress-strain curves for the crumpled-based scaffolds with a porosity (Π) of **a.** 75%, **b.** 80% and **c.** 85%, made of elements with a triangular (red), square (yellow), pentagonal (blue) or circular (green) base geometries combined with an armlength of 8, 12 or 16mm. The error bars in **b.** describe the standard deviation.*

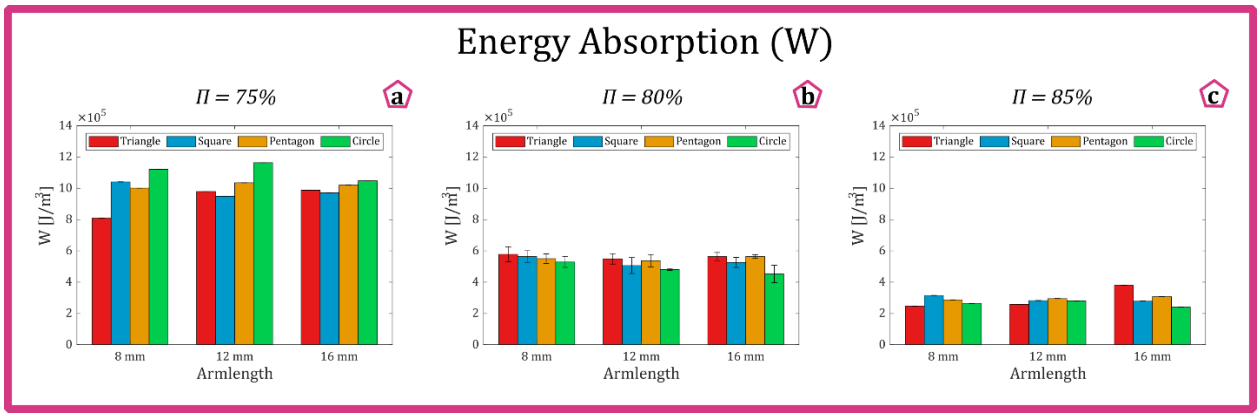

*Figure 3-5: The energy absorption (W) calculated at the applied strain of 0.5 for the crumpled-based scaffolds with a porosity level of **a.** 75%, **b.** 80% and **c.** 85%, made of elements with a triangular (red), square (yellow), pentagonal (blue) or circular (green) base combined with an armlength of 8, 12 or 16mm.*

The difference between the porosities was seen in the initial elastic stiffness as well. Figure 3-4 shows the initial elastic stiffness of all different groups. The initial elastic stiffness in crumpled-based scaffolds with a porosity of 80% seems to be comparable, independent of the geometry of the scaffold elements. However, in the scaffolds with a porosity of 75%, differences in the initial elastic stiffness between different element geometries were observed. The scaffolds made of elements with a circular base and arms of 8 and 12 mm were higher (i.e., about 1.5 MPa) than the initial elastic stiffness in the other scaffolds with the same level of porosities. The absolute differences in initial elastic stiffness in crumpled-based scaffolds with a porosity of 85% were smaller(i.e., about 1 MPa), however, the relative difference is much higher, as the values of the initial stiffness are lower.

The differences between the porosities were visible in the amount of energy absorbed by the crumpled-based scaffold as well (Figure 3-5). Under the value of applied strains (i.e. 50%) scaffolds with a higher porosity absorbed less energy than those with lower porosity. The difference between the scaffolds with a porosity of 85% and the scaffolds with a porosity of 80% was in the range of 2-4 × 10^5 J/m^3. The difference between the scaffolds with a porosity of 80% and the scaffolds with a porosity of 75% was in the range of 2-5 × 10^5 J/m^3. Differences between scaffolds with the same porosity but different element designs were smaller (circa 1 × 10^5 J/m^3). In crumpled-based scaffolds with a porosity of 75%, The larger differences were seen in scaffolds made of elements with armlengths of 8 and 12 mm, while in scaffolds with a porosity of 85% the larger differences were seen in the scaffolds made of elements with armlengths of 16 mm.

3.4 Relationship between morphological and mechanical properties

Figure 3-6 shows the development of the mean pore size in the crumpled-based scaffolds made of elements with a pentagon base, and armlengths of respectively 8, 12 and 16 mm. The mean pore size in scaffolds made of elements with an armlength of 8 mm and the elements with an armlength of 12 and 16 mm was slightly smaller (about 0.1 mm). The decrease in the mean pore size was similar in all three scaffolds with the same base geometries, but different arm lengths. However, in all samples, the standard deviation was rather large (about 2,5 mm to 2.0 mm). The standard deviation was the smallest in the scaffold made out of elements with an armlength of 8 mm.

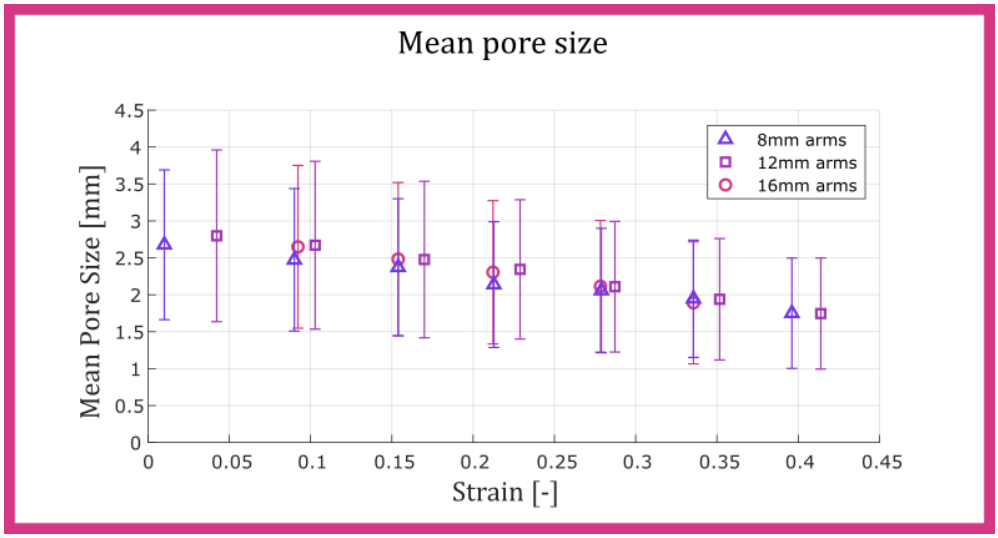

Figure 3-6: The mean pore size and standard deviation during compression in crumpled-based scaffolds with a pentagonal base and armlengths of 8, 12 and 16 mm starting with a porosity of 80%.

Figure 3-7 shows the initial elastic stiffness vs the porosity per base geometry. The armlengths of the elements in the crumpled-based scaffold seem to slightly affect the initial elastic stiffness of the scaffold. Scaffolds with a porosity of 75% showed that the initial elastic stiffness in scaffolds made of elements with armlengths of 16 mm is lower than scaffolds made of elements with armlengths of 12 and 8 mm. The scaffolds made of elements with armlengths of 8 mm show the highest initial elastic stiffness. This applies to all different base geometries. However, the absolute differences between armlengths are dissimilar in all base geometries. In the other porosities (i.e., 80% and 85%), there is no uniform order of armlength in comparison to the initial elastic stiffness.

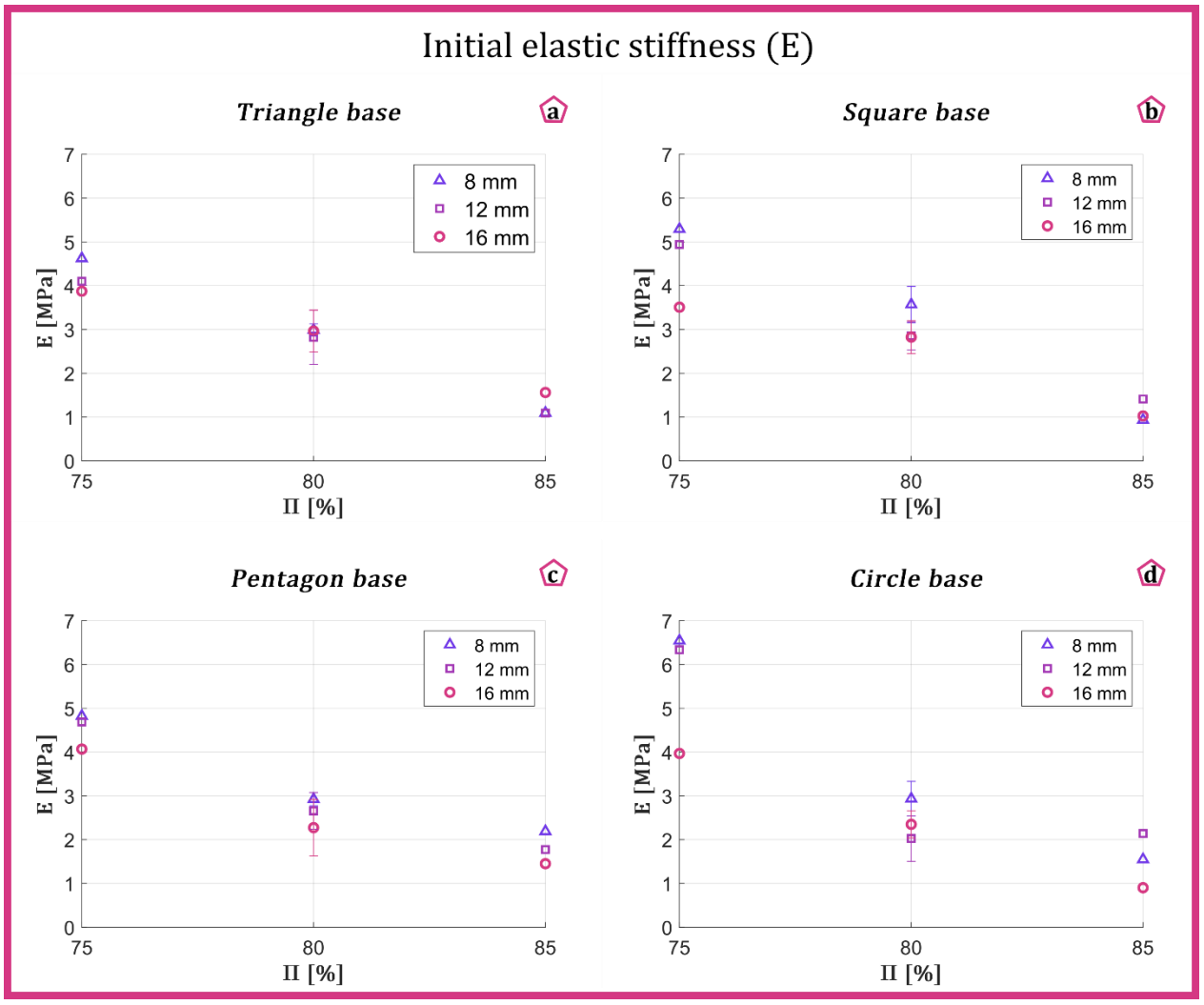

*Figure 3-7: The initial elastic stiffness (E) calculated from the stress-strain curves for the crumpled-based scaffolds made of elements with a **a.** triangular, **b.** square, **c.** pentagonal or **d.** circular base geometry plotted against porosity(Π).*

The evolution of the elastic stiffness during compression is shown in Figure 3-8. Since the porosity of the scaffold is superior to the geometry of the elements in affecting the initial elastic stiffness, all scaffolds with the same porosity were combined and the mean and standard deviation were calculated. To assess if the initial density will influence the elastic stiffness, the elastic stiffness was plotted against the relative density. The elastic stiffness at a given relative density seems to be slightly higher (about 0.5 MPa) when the initial relative density was lower.

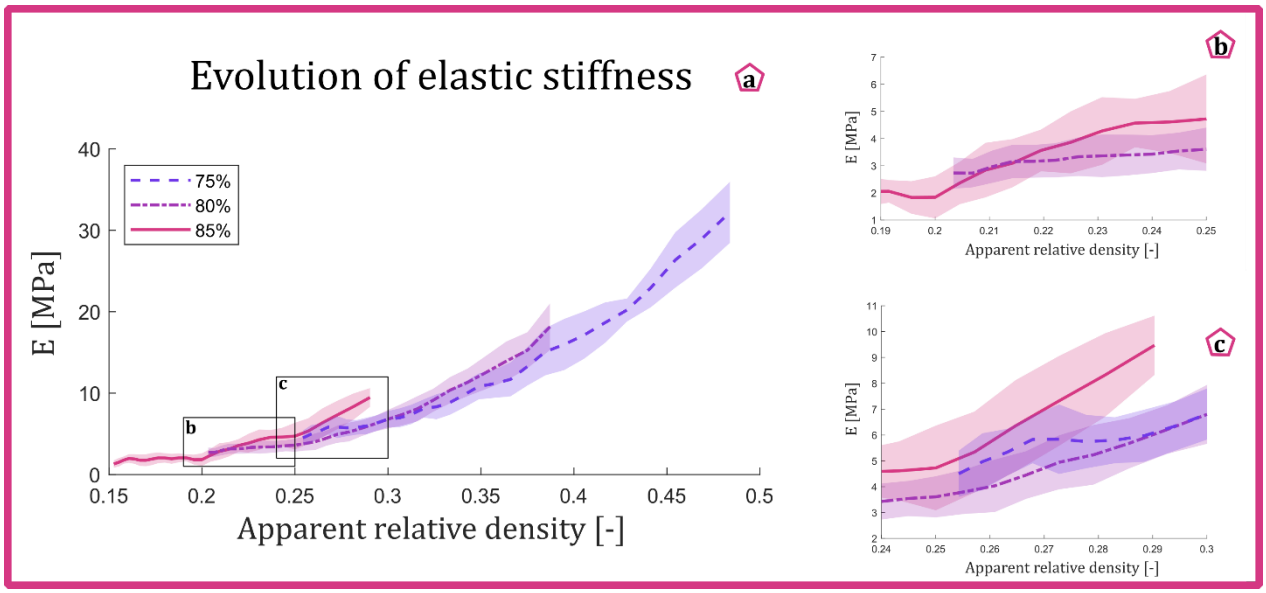

Figure 3-8: ***a.*** *The evolution of the elastic stiffness against the relative density for all scaffolds, regardless of the element geometry, with the porosity (Π) of 75% (blue), 80% (purple) and 85% (pink). The line shows the average of all different scaffolds within the porosity group, and the coloured patch shows the standard deviation.* ***b.*** *A zoom-in image of subpanel b in the sub-figure a.* ***c.*** *A zoom-in image of subpanel c in the sub-figure a.*

4. Discussion

This thesis aimed to design, fabricate and characterize crumpled-based meta-biomaterials as bone filling substituents. In this thesis, the possibility to create a crumpled-based scaffold from separate elements made from a shape memory material has been shown. The methodology described here for assembling the scaffold was based on crumpling, resulting in scaffolds with disordered microstructures which will be consequently less sensitive to defects as compared to other types of porous scaffolds made by other techniques such as origami-based scaffolds [13]. Furthermore, when the design is based on crumpling, the initial design is easy to create. The costs will be low in comparison to other techniques to create porous scaffolds, such as origami-based scaffolds, in which the initial design needs to be very precise. The advantage of crumpling is that the way it is crumpled has little effect on the final structure and the mechanical and morphological properties of the final structure [13].

The first research question mentioned in the introduction was: "Can crumpling be used as a technique to create a porous scaffold in a way that is reproducible?" The crumpled-based scaffold created in this thesis shows that crumpling can be used as a technique to create a porous scaffold. Different base geometries were used to build the scaffold. In the category of scaffolds with a porosity of 80% three scaffolds were made per base geometry, to determine if the technique is reproducible. The stress-strain curves in Figure 3-3 show that the curves for scaffolds with the same base geometry were similar, which shows the reproducibility of the crumpled-based scaffold.

The second research question was: "How to use smart materials (e.g., shape memory polymers) as a building block of crumpled-based meta-biomaterials, by making separate crumpled elements and combining them with the use of arbitrary shape changes?". We started by 3D printing separate flat elements made of the shape memory material PLA, programming the material with the original flat shape. By heating the elements above the glass temperature and crumpling the elements afterwards, the temporary 3D shape was set. Then, several elements were put in a confined space and heated above the glass temperature again, which triggered the element to go back to their original flat shape. As the space was confined and there was not enough space for the elements to completely go back to their original flat shape, they tangled and a crumpled-based scaffold was created.

As this method allows to build a scaffold from separate small crumpled elements, it will be applicable through minimally invasive surgery, which will have a positive effect on the healing process of the patient. The healing will be quicker, there will be less chance of infection or other complications and it will stimulate the body to heal by itself without the use of donor material.

4.1 Morphological properties

Longitudinal cross-sections of the scaffolds during compression confirm only densification takes place. No fractures were seen in the scaffolds during or after compression. During compression, the number of contacts increased and the spacing between elements decreased. This behaviour was similar to the mechanics of entangled materials without crosslinks [57], but also similar to crumpled materials [13], which could be explained by the fact that the scaffolds were built out of crumpled elements.

Pore sizes in a porous scaffold are very important to provide oxygen and nutrient supply to facilitate vascularisation and bone growth [61]. The dimension of osteoblasts is in a range of 10 to 50µm [62]. However, to regenerate bone tissue the pore size of the scaffold needs to be much higher. It has been shown that pores >300µm are essential to promote osteoinductivity by facilitating vascularization [61-63]. Smaller pore sizes stimulate cell attachment in scaffolds because the specific surface area is higher. However, when cells attach, there is less space available for cell infiltration and cell migration into the scaffold [63].

The measurements of mean pore sizes between elements in scaffolds built out of elements with a pentagonal base show a small difference in mean spacing for different armlengths. Elements with longer arms tend to create a larger mean spacing than elements with shorter arms. Where elements with shorter arms can just get closer to each other, elements with longer arms need to buckle more during compressing, which requires more space. After compression, all scaffolds show a smaller pore size. The porosity is lower after compression, therefore, less space is available for the elements and the spacing between the elements will become smaller. After compression, there appears to be a small difference between the elements with shorter and longer arms as well.

Table 3-1 shows that the mean spacing in the scaffold created from elements with an armlength of 8 mm is similar to the mean spacing in the scaffold created from elements with an armlength of 12 mm. However, the first scaffold is less compressed as the porosity is 68.1%, while the porosity of the scaffold created from elements with an armlength of 12 mm is compressed to a porosity of 64.5%. This means that the scaffolds created from elements of 8 mm will reach the same pore sizes at a higher porosity.

The mean pore sizes in our scaffolds are rather large in comparison to other studies [64]. In bone tissue engineering pore sizes of 20 to 1500 µm are used, and the optimum pore size is 300µm or higher [63, 64]. In our scaffolds, the mean pore size is much higher. However, as can be seen in Figure 3-2, the size of the pores varies throughout the scaffold. Due to the crumpling method, the scaffold is highly heterogeneous, which could combine the characteristics of the smaller pores, cell attachment, and the larger pores, vascularisation, cell infiltration and cell migration.

4.2 Mechanical properties

The stress-strain curves (Figure 3-3) derived from the confined compression tests showed similar stress-strain trends to those of entangled materials without a structural connection (crosslinks) between the separate elements. They show no fraction, only densification. This could be due to the fact that the scaffold consisted of separate elements, which can rearrange under pressure, preventing fracture [57].

The third research question mentioned in the introduction of this thesis was: “Does the geometry of the separate elements, used to create the scaffold, influence the mechanical properties of the fabricated scaffold?” Four different base geometries of the elements and three different armlengths were used to determine if there would be any effect on the mechanical properties. To check the reproducibility of the mechanical test, 3 scaffolds of each element design with a porosity of 80% were mechanically tested. The mechanical tests showed that there was only a small difference in the stress-strain curves of the scaffolds containing elements with different geometries. Neither the number of arms, nor the length of the arms seemed to greatly affect the macroscopic mechanical properties of the crumpled-based scaffolds. The shape of the curve in the stress-strain diagrams is comparable for all designs. This is due to the rearrangement of the elements during compression [53].

The initial elastic stiffness in the crumpled-based scaffolds with a porosity of 80% doesn't seem to be widely affected by the geometry of the elements (Figure 3-4b). The initial elastic stiffness for all scaffolds stayed between 2.5 and 3.5 MPa. In the group with armlengths of 8mm, the square base has a slightly higher initial stiffness (about 0.5 MPa), than the other base geometries in that group. In the group of scaffolds with an armlength of 12mm, the scaffolds with a circular base geometry had a lower initial stiffness (about 0.5 MPa) than the scaffolds with other base geometries. In the last group with armlengths of 16 mm, the scaffolds with a triangular and square base geometries showed a higher initial elastic stiffness (about 0.5 MPa). This leads to the conclusion that the crumpled-based scaffolds with a square base geometry had the highest resistance to elastic deformation and the crumpled-based scaffolds with a circular base geometry had the lowest resistance to elastic deformation. However, the difference is small and the sample size was only three. To be able to make this conclusion, the tests need to be done with a larger sample size.

In the groups with other porosities (Figure 3-4a and c) the differences in initial elastic stiffness between the base geometries were larger. In the scaffolds with a porosity of 75%, the scaffolds made of elements with a circular base and armlengths of 8 and 12 showed a higher initial elastic stiffness (i.e., about 1.5 MPa) than the scaffolds made of elements with other base geometries. The absolute differences in the scaffolds with a porosity of 85% were smaller, but as the values of the initial elastic stiffness were smaller, the relative differences were much higher. However, the sample size in the groups with a porosity of 75% and 85%, was only 1. Therefore it is not clear if the observed differences are due to the differences in base geometries or within the range of natural standard deviation between samples. More tests should be done to determine the origin of the differences.

What does become clear in Figure 3-4, is the influence of the porosity on the initial elastic stiffness. The initial elastic stiffness was higher when the initial porosity was lower. This means the elastic stiffness can be tuned by altering the porosity so it can mimic the elastic stiffness of the tissue it should rebuild.

The energy absorption during the compression tests shows that it was dependent on the porosity as well (Figure 3-5). The crumpled-based scaffolds with higher porosities absorbed less energy at the applied strain level of 50% as compared to those with lower porosities. The difference between the scaffolds with a porosity of 85% and the scaffolds with a porosity of 80% was in the range of 2-4 × 10^5 J/m3. The difference between the scaffolds with a porosity of 80% and the scaffolds with a porosity of 75% was in the range of 2-5 × 10^5 J/m3. None of the scaffolds fractured during the compression tests, likely because of rearranging of the elements within the scaffold as well as adjusting local bending or buckling deformation of the elements, therefore reducing stress concentration at the ridges (folds) by creating new ridges and alternating the flow of deformation within the structure [65, 66]. This densification process results in higher resistance to stresses in scaffolds with lower porosity. Therefore more energy will be absorbed by scaffolds with lower porosities.

Differences in energy absorption between scaffolds with the same porosity but different element designs were smaller (circa 1 × 10^5 J/m3). Interestingly, scaffolds with a porosity of 75%, showed larger differences in scaffolds made out of base geometries with armlengths of 8 and 12 mm, while scaffolds with a porosity of 85% showed larger differences in scaffolds made out of base geometries with armlengths of 16 mm. This could be due to the possibility of forming new ridges. During early stages of crumpling, new ridges will be created, which will be able to store energy [13]. Throughout further compaction, the space to form new ridges will become smaller. Fewer ridges will be formed, therefore less additional energy will be stored. In the scaffolds with a porosity of 75%, there is less room to create new ridges. Elements with armlengths of 16 mm need more space to create new ridges, than the elements with armlengths of 8 or

12 mm. When no sufficient space is available, no new ridges will be formed during further compaction, and therefore the energy stored will remain similar and differences in energy storage between different scaffolds will be smaller.

4.3 Relationship between morphological and mechanical properties

The last research question stated in the introduction of this thesis was: "Does the initial porosity of the scaffold affect the mechanical and morphological properties?". Porosity affected the mechanical and morphological properties, which was expected. The more material is in the scaffold, the harder it will be to compress the scaffold, depending on the properties of the shape memory material from which the elements were made. Additionally, the mean pore size will decrease as well, when the porosity decreases. Less space will be available and therefore the pores will become smaller.

Figure 3-6 shows that the decrease in the mean pore size was similar in three scaffolds with the same base geometries, but different arm lengths. However, in all samples, the standard deviation was rather large (about 2,5 mm to 2.0 mm). This could be explained by the fact that the scaffolds are based on crumpling, which results in a highly heterogeneous structure. As stated before this could combine the characteristics of the smaller pores, cell attachment, and the larger pores, vascularisation, cell infiltration and cell migration. However, Figure 3-6 shows that the standard deviation of the mean pore size is not reaching the sizes which are needed for the smaller pores to promote cell attachment. Furthermore, the mean pore size is much bigger than the pore sizes used in other studies of scaffolds. By lowering the mean pore sizes the scaffolds could be optimized to facilitate what is needed. Figure 3-6 shows that with compression the mean pore size becomes smaller. After a height reduction of 7 mm, the mean pore size is lowered by approximately 1 mm. Another way to reduce the mean pore size might be to create a scaffold out of smaller elements. Then a scaffold with a similar porosity but smaller pore sizes could be obtained.

As discussed in the previous section, the initial elastic stiffness is dependent on the porosity as well. In Figure 3-7 the initial elastic stiffness is plotted against the porosity for each base geometry. It shows that in scaffolds with a porosity of 75% the scaffolds made of elements with armlengths of 8 mm exhibit the highest initial elastic stiffness. This applies to all different base geometries. However, the absolute differences between armlengths are dissimilar in all base geometries. This could be due to the small sample size or depend on the base geometry. To know for sure which is the actual cause of the differences, more tests should be done. In the other porosities (i.e., 80% and 85%), there is no uniform order of armlength in comparison to the initial elastic stiffness.

4.4 Future research

When the created scaffolds will be used as a scaffold for tissue-engineered bone, the scaffold needs to have sufficient compressive strength to support the body weight [61]. Also, the elastic stiffness of the scaffold needs to be within the range of elastic stiffness of cancellous bone (which ranges from 0.01 to 3.0 GPa). This will be higher for the cortical bone which ranges from 4.4 GPa to 28.8 GPa [67, 68]. Given the elastic stiffness of the crumpled-based scaffolds proposed here, they suggest that the current scaffold designs would be appropriate for replacing biomaterials to fill in the bone and replace the damaged bony tissue. However, to be able to use the scaffolds in a human body, further research is needed.

As stated before, the method used to create this crumpled-based scaffold is applicable in minimally invasive surgery. We suggest exploring the use of other shape-memory materials, with a stimulus which is less damaging to the human body. The stimulus of PLA is heat, and for the best outcome, it needs to be heated to at least 80 degrees Celsius, which is harmful to the surrounding tissue in the human body. A

shape memory material stimulated by magnetism, light, moisture or change in pH value could be better suited [69]. However, instead of looking for another material, the altering of this material could be a solution to the problem as well. The way the material is heated could be optimized, so the heating is very localized. If metallic particles are added to the material, the heat needed for the material to shift shape could be obtained from friction by using magnetism. The polymer could also be altered to lower the temperature needed for activation of the material, so it will be less damaging to the surrounding tissue.

Future studies can focus on optimizing pore sizes. As mentioned before, the pore sizes of the scaffolds built in this study are higher than the pore sizes which are considered optimal. The pore sizes could be decreased by compressing the scaffolds and use of lower porosity. However, a lower porosity is not always preferred. Therefore, future research could also look into the use of smaller elements to build a scaffold.

Furthermore, the permeability should be investigated, to make sure the pores are interconnected, and nutrients and oxygen can easily flow through the scaffold to stimulate cell growth. To stimulate cell growth even more, nanopatterns could be applied on the surface of the elements. As the elements start from a 2D state, existing techniques could be used for this. This could not only stimulate cell growth but also prevent the growth of bacteria [8]. In addition, drug delivery could be incorporated in the scaffold as well.

5. CONCLUSION

This thesis aimed to design, fabricate and characterize crumpled-based meta-biomaterials as bone filling substituents. In this thesis, it has been shown that building a crumpled-based scaffold using separate elements made of a shape memory material is feasible. Compression tests showed the scaffolds didn't fracture during compression. They densified, showing similar behaviour as entangled materials. The different geometries of the elements used in this study did affect the mechanical properties in a small way. However, different porosities showed larger differences in resistance to compression. The denser the material the higher the resistance. The elastic stiffness was higher when the porosity was lower. Therefore, the porosity of the crumpled-based scaffold can tune mechanical properties. The properties of bone could be mimicked to make it possible for the scaffold to be used as bone filling substituents.

The micro-CT showed that the mean pore size was also dependent on the porosity. The lower the porosity, the smaller the mean pore sizes were. However, the pore sizes were rather large in comparison to other studies in which scaffolds are studied. Therefore it is recommended to research this way of creating scaffolds further. To optimize the properties and study the effects on cell growth.

6. REFERENCES

1. Keeney, M., et al., *Tissue engineering: focus on the musculoskeletal system.* Biomaterials Science; Rosen, Y., Elman, N., Eds, 2012: p. 191-221.
2. Tanaka, M., et al., *A three-dimensional block structure consisting exclusively of carbon nanotubes serving as bone regeneration scaffold and as bone defect filler.* PLoS One, 2017. **12**(2): p. e0172601.
3. Chen, G., T. Ushida, and T. Tateishi, *Scaffold design for tissue engineering.* Macromolecular Bioscience, 2002. **2**(2): p. 67-77.
4. Montgomery, M., et al., *A Method for the Fabrication of Elastomeric Polyester Scaffolds for Tissue Engineering and Minimally Invasive Delivery.* ACS Biomaterials Science & Engineering, 2018.
5. Liu, X. and P.X. Ma, *Polymeric scaffolds for bone tissue engineering.* Annals of biomedical engineering, 2004. **32**(3): p. 477-486.
6. Stratton, S., et al., *Bioactive polymeric scaffolds for tissue engineering.* Bioactive materials, 2016. **1**(2): p. 93-108.
7. Mathieu, L.M., et al., *Architecture and properties of anisotropic polymer composite scaffolds for bone tissue engineering.* Biomaterials, 2006. **27**(6): p. 905-916.
8. Hasan, J., R.J. Crawford, and E.P. Ivanova, *Antibacterial surfaces: the quest for a new generation of biomaterials.* Trends in biotechnology, 2013. **31**(5): p. 295-304.
9. Martinez, E., et al., *Effects of artificial micro-and nano-structured surfaces on cell behaviour.* Annals of Anatomy-Anatomischer Anzeiger, 2009. **191**(1): p. 126-135.
10. Yim, E.K., S.W. Pang, and K.W. Leong, *Synthetic nanostructures inducing differentiation of human mesenchymal stem cells into neuronal lineage.* Experimental cell research, 2007. **313**(9): p. 1820-1829.
11. Yim, E.K., et al., *Nanopattern-induced changes in morphology and motility of smooth muscle cells.* Biomaterials, 2005. **26**(26): p. 5405-5413.
12. Neuhuber, B., et al., *Reevaluation of in vitro differentiation protocols for bone marrow stromal cells: disruption of actin cytoskeleton induces rapid morphological changes and mimics neuronal phenotype.* Journal of neuroscience research, 2004. **77**(2): p. 192-204.
13. Fokker, M., S. Janbaz, and A. Zadpoor, *Crumpling of thin sheets as a basis for creating mechanical metamaterials.* RSC advances, 2019. **9**(9): p. 5174-5188.
14. Kundu, S., et al., *Crumpled sheets of reduced graphene oxide as a highly sensitive, robust and versatile strain/pressure sensor.* Nanoscale, 2017. **9**(27): p. 9581-9588.
15. Luo, J., et al., *Crumpled graphene-encapsulated Si nanoparticles for lithium ion battery anodes.* The journal of physical chemistry letters, 2012. **3**(13): p. 1824-1829.
16. Dou, X., et al., *Self-dispersed crumpled graphene balls in oil for friction and wear reduction.* Proceedings of the National Academy of Sciences, 2016. **113**(6): p. 1528-1533.
17. Choi, J., et al., *Hierarchical, dual-scale structures of atomically thin MoS2 for tunable wetting.* Nano letters, 2017. **17**(3): p. 1756-1761.
18. Song, J., et al., *Superflexible wood.* ACS applied materials & interfaces, 2017. **9**(28): p. 23520-23527.
19. Werner, M., et al., *Surface curvature differentially regulates stem cell migration and differentiation via altered attachment morphology and nuclear deformation.* Advanced science, 2017. **4**(2): p. 1600347.
20. Randall, C.L., E. Gultepe, and D.H. Gracias, *Self-folding devices and materials for biomedical applications.* Trends in biotechnology, 2012. **30**(3): p. 138-146.

21. van Manen, T., S. Janbaz, and A.A. Zadpoor, *Programming 2D/3D shape-shifting with hobbyist 3D printers.* Materials Horizons, 2017.
22. Vasiev, I., et al., *Self-folding nano-and micropatterned hydrogel tissue engineering scaffolds by single step photolithographic process.* Microelectronic Engineering, 2013. **108**: p. 76-81.
23. Janbaz, S., et al., *Origami lattices with free-form surface ornaments.* Science advances, 2017. **3**(11): p. eaao1595.
24. T. van Manen, S.J., Amir A. Zadpoor, *Programming the shape-shifting of flat soft matter.* 2017.
25. Janbaz, S., R. Hedayati, and A. Zadpoor, *Programming the shape-shifting of flat soft matter: from self-rolling/self-twisting materials to self-folding origami.* Materials Horizons, 2016. **3**(6): p. 536-547.
26. Baimova, J., et al., *Review on crumpled graphene: unique mechanical properties.* Reviews on Advanced Materials Science, 2014. **39**(1).
27. Mirzaali, M.J., et al., *Crumpling-based soft metamaterials: the effects of sheet pore size and porosity.* Sci Rep, 2017. **7**(1): p. 13028.
28. Cottrino, S., et al., *Mechanical properties of crumpled aluminum foils.* Acta Materialia, 2014. **81**: p. 98-110.
29. Bouaziz, O., et al., *Compression of crumpled aluminum thin foils and comparison with other cellular materials.* Materials Science and Engineering: A, 2013. **570**: p. 1-7.
30. Lin, Y.-C., et al., *Spontaneous emergence of ordered phases in crumpled sheets.* Physical review letters, 2009. **103**(26): p. 263902.
31. Deboeuf, S., et al., *Comparative study of crumpling and folding of thin sheets.* Physical review letters, 2013. **110**(10): p. 104301.
32. Matan, K., et al., *Crumpling a thin sheet.* Physical Review Letters, 2002. **88**(7): p. 076101.
33. Vliegenthart, G. and G. Gompper, *Forced crumpling of self-avoiding elastic sheets.* Nature Materials, 2006. **5**(3): p. 216-221.
34. Balankin, A.S. and O.S. Huerta, *Entropic rigidity of a crumpling network in a randomly folded thin sheet.* Physical Review E, 2008. **77**(5): p. 051124.
35. Susarrey Huerta, O., et al. *Mechanics of randomly folded thin materials*. in *Advanced Materials Research*. 2009. Trans Tech Publ.
36. Hanaor, D., et al., *Mechanical properties in crumple-formed paper derived materials subjected to compression.* Heliyon, 2017. **3**(6): p. e00329.
37. Kolken, H.M. and A. Zadpoor, *Auxetic mechanical metamaterials.* RSC Advances, 2017. **7**(9): p. 5111-5129.
38. Hager, M.D.e.a., *Shape memory polymers: Past, present and future developments.* Progress in Polymer Science, 2015. **49**(50): p. 3-33.
39. Zhao, Q., H.J. Qi, and T. Xie, *Recent progress in shape memory polymer: New behavior, enabling materials, and mechanistic understanding.* Progress in Polymer Science, 2015. **49**: p. 79-120.
40. Meng, H. and G. Li, *A review of stimuli-responsive shape memory polymer composites.* Polymer, 2013. **54**(9): p. 2199-2221.
41. Huang, W., et al., *Shape memory materials.* Materials Today, 2010. **13**(7): p. 54-61.
42. Lendlein, A. and R. Langer, *Biodegradable, elastic shape-memory polymers for potential biomedical applications.* Science, 2002. **296**(5573): p. 1673-1676.
43. Hinds, S.A. and S.E. Feinberg, *Tissue Engineering as a Minimally Invasive Method*, in *Minimally Invasive Oral and Maxillofacial Surgery*, O. Nahlieli, Editor. 2018, Springer Berlin Heidelberg: Berlin, Heidelberg. p. 185-197.
44. Farah, S., D.G. Anderson, and R. Langer, *Physical and mechanical properties of PLA, and their functions in widespread applications—A comprehensive review.* Advanced drug delivery reviews, 2016. **107**: p. 367-392.

45. Inoue, K., M. Yamashiro, and M. Iji, *Recyclable shape-memory polymer: Poly (lactic acid) crosslinked by a thermoreversible Diels–Alder reaction.* Journal of Applied Polymer Science, 2009. **112**(2): p. 876-885.
46. Yamashiro, M., K. Inoue, and M. Iji, *Recyclable shape-memory and mechanical strength of poly (lactic acid) compounds cross-linked by thermo-reversible Diels-Alder reaction.* Polymer journal, 2008. **40**(7): p. 657.
47. Karageorgiou, V. and D. Kaplan, *Porosity of 3D biomaterial scaffolds and osteogenesis.* Biomaterials, 2005. **26**(27): p. 5474-5491.
48. Hu, Y., et al., *Fabrication of poly (α-hydroxy acid) foam scaffolds using multiple solvent systems.* Journal of Biomedical Materials Research Part A, 2002. **59**(3): p. 563-572.
49. Maspero, F., et al., *Resorbable defect analog PLGA scaffolds using CO2 as solvent: structural characterization.* Journal of Biomedical Materials Research Part A, 2002. **62**(1): p. 89-98.
50. Ozturk, U.E. and G. Anlas, *Energy absorption calculations in multiple compressive loading of polymeric foams.* Materials & Design, 2009. **30**(1): p. 15-22.
51. Schindelin, J., et al., *Fiji: an open-source platform for biological-image analysis.* Nature methods, 2012. **9**(7): p. 676-682.
52. Doube, M., et al., *BoneJ: free and extensible bone image analysis in ImageJ.* Bone, 2010. **47**(6): p. 1076-1079.
53. Mezeix, L., et al., *Mechanical behavior of entangled fibers and entangled cross-linked fibers during compression.* Journal of materials science, 2009. **44**(14): p. 3652-3661.
54. Gadot, B., et al., *Entangled single-wire NiTi material: A porous metal with tunable superelastic and shape memory properties.* Acta Materialia, 2015. **96**: p. 311-323.
55. Rodney, D., et al., *Reversible dilatancy in entangled single-wire materials.* Nature materials, 2016. **15**(1): p. 72.
56. Picu, R., *Mechanics of random fiber networks—a review.* Soft Matter, 2011. **7**(15): p. 6768-6785.
57. Masse, J.-P. and D. Poquillon, *Mechanical behavior of entangled materials with or without cross-linked fibers.* Scripta Materialia, 2013. **68**(1): p. 39-43.
58. Li, Q., I. Magkiriadis, and J.J. Harrigan, *Compressive strain at the onset of densification of cellular solids.* Journal of cellular plastics, 2006. **42**(5): p. 371-392.
59. Liu, P., et al., *Compressive and pseudo-elastic hysteresis behavior of entangled titanium wire materials.* Materials Science and Engineering: A, 2010. **527**(15): p. 3301-3309.
60. Tan, Q., et al., *Mechanical behaviors of quasi-ordered entangled aluminum alloy wire material.* Materials Science and Engineering: A, 2009. **527**(1-2): p. 38-44.
61. Collins, M.N., et al., *Scaffold fabrication technologies and structure/function properties in bone tissue engineering.* Advanced Functional Materials, 2021. **31**(21): p. 2010609.
62. Abbasi, N., et al., *Porous scaffolds for bone regeneration.* Journal of Science: Advanced Materials and Devices, 2020. **5**(1): p. 1-9.
63. Murphy, C.M., M.G. Haugh, and F.J. O'brien, *The effect of mean pore size on cell attachment, proliferation and migration in collagen–glycosaminoglycan scaffolds for bone tissue engineering.* Biomaterials, 2010. **31**(3): p. 461-466.
64. Loh, Q.L. and C. Choong, *Three-dimensional scaffolds for tissue engineering applications: role of porosity and pore size.* 2013.
65. Liu, Y., et al., *Early plastic deformation behaviour and energy absorption in porous β-type biomedical titanium produced by selective laser melting.* Scripta Materialia, 2018. **153**: p. 99-103.
66. Wang, D., *Impact behavior and energy absorption of paper honeycomb sandwich panels.* International Journal of Impact Engineering, 2009. **36**(1): p. 110-114.
67. Geetha, M., et al., *Ti based biomaterials, the ultimate choice for orthopaedic implants–a review.* Progress in materials science, 2009. **54**(3): p. 397-425.

68. He, G., P. Liu, and Q. Tan, *Porous titanium materials with entangled wire structure for load-bearing biomedical applications.* Journal of the mechanical behavior of biomedical materials, 2012. **5**(1): p. 16-31.
69. Delaey, J., P. Dubruel, and S. Van Vlierberghe, *Shape-memory polymers for biomedical applications.* Advanced Functional Materials, 2020. **30**(44): p. 1909047.

APPENDICES

APPENDIX A: EVOLUTION OF ELASTIC STIFFNESS

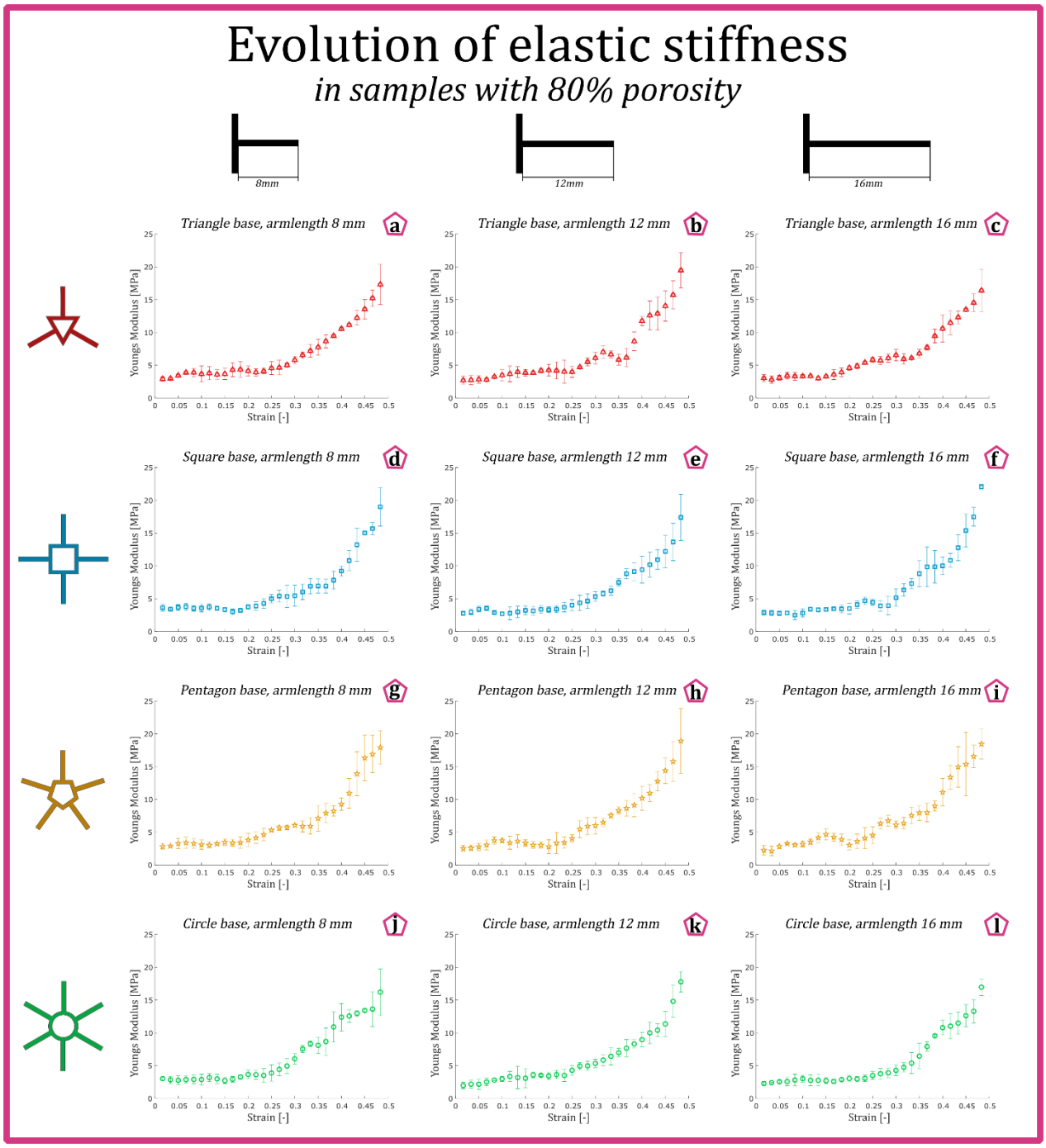

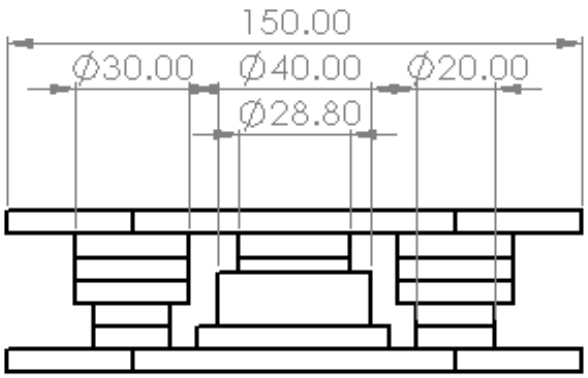

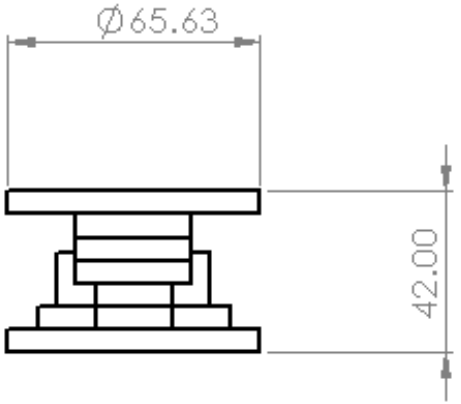

		UNLESS OTHERWISE SPECIFIED:		NAME	DATE
		DIMENSIONS ARE IN MILLIMETERS	DRAWN		
			CHECKED		
			ENG APPR.		
			MFG APPR.		
		INTERPRET GEOMETRIC TOLERANCING PER:	Q.A.		
		MATERIAL	COMMENTS:		
NEXT ASSY	USED ON	FINISH			
APPLICATION		DO NOT SCALE DRAWING			

PROPRIETARY AND CONFIDENTIAL

TU Delft

TITLE:
SCHEMATIC REPRESENTATION OF THE HOLDER

SIZE	DWG. NO.	REV
A	1	

SHEET 1 OF 1